Chapter 16

RADIOMETRIC AND GEOMETRIC INFORMATION CONTENT OF TiungSAT-1 MSEIS DATA

Mazlan Hashim & Wan Hazli Wan Kadir
Faculty of Geoinformation Science and Engineering
Universiti Teknologi Malaysia

INTRODUCTION

In the last two decades, satellite remote sensed data have been widely used for assisting natural resource management and environmental protection works. In both application areas, there are various level of utilisation of remote sensing techniques. In most developed nations such techniques have been in place as an operational tool while in most developing countries efforts are still underway to establish operational applications. This includes Malaysia, where remote sensing applications at user agencies are still at the semi-operational level due to various reasons. In the context of Malaysia, (in the late 70's to early 90's) the hindering factors can be categorised into : (1) lack of infrastructure and facilities to enable such applications of the technology to be optimised, and (2) lack of expertise within relevant organisations that enables them to undertake such applications. The former factor is now completely addressed with the government's emphasis on provide computing facilities within all user agencies, and in fact most of the relevant agencies already have minimum capacity to process satellite remote sensing data for specific applications. The latter is an on-going process within all relevant agencies where programmes to train personnel to the expert level are carried out as a long term commitment.

Apart from the above factors, the application of remote sensing technique is also very much dependent on the inherent parameters of the data, namely the spatial, spectral and temporal resolutions.

The spatial resolution dictates the degree of information content within data recorded by the sensor, hence, determining the scale of information that can be derived. The finer the spatial resolution, the more spatial information is contained in the data. Similarly, the lower the resolution, the less information will be contained in the data but the spatial elements are still inherent within the data. The spatial data in low spatial resolution data are often associated with textures and can be extracted by texture descriptors. Visually, textures are viewed as tonal rendition found in an image and can also associated with colour when colour composites are viewed in the red-green-blue guns of the display system. Tone or textures play a remarkably important role in recognising patterns from remote sensing data, where in most cases texture provides better class delineation in the image when classified digitally.

The temporal resolution of the data is very important when the data is to be used for analysing changes within the same data set in a given specified time frame. Other than change detection analysis, temporal data sets acquired closed to each other can optimise the delineation of subtle classes, thus improving classification of data. However, obtaining temporal data set over the same scene using a passive system is not very likely in humid tropic regions like Malaysia due to high probability of cloud cover throughout the year.

The data spectral resolution is crucial in determining the sensitivity of the data recorded as the spectral responses within specified bands are able to differentiate targets of interest. The finer spectral resolution is often associated with the width of each of the spectral band or the numbers of bands that exist in the system. The narrow bandwidth would be very sensitive to certain targets thereby resulting in better delineation among them, but this is only valid in non-thermal bands where a larger bandwidth is needed to sense the emission. The number of bands can be viewed as a number of observations for a given area. The larger the number of observations, the better it is statistically, to estimate the most probable value of all targets, hence making possible the extraction of information from these data.

In practice, only the spatial and spectral resolutions are of much concern when remote sensing data is used, and it is referred to as geometric and radiometric information. To enable particular applications to be carried out using certain remote data, both the radiometric and geometric information must be contained in the data. Within this context, this paper examines both the radiometric and geometric information of the Multi-Spectral Earth Imaging System (MSEIS) onboard TiungSAT-1. The MSEIS operates with visible bands at approximately 78m spatial resolution.

MATERIAL AND METHOD

MSEIS System

The MSEIS system comprises three narrow angle cameras (NAC) in three spectral bands. Each camera is electrically identical and it includes support chip, video ADC image buffer memory and communication interfaces. TiungSAT-1's MSEIS can collect maximum 4 images contiguously along the flight path. These images will need to be compressed and transferred to the onboard computer (OBC) before the imaging system

can perform any subsequent imaging task. The duration between one imaging task and the other is dependent on the number of images that has to be compressed and transferred to the OBC.

The salient parameters of MSEIS that is of interest in the paper is given in Table 1. Apart from the MSEIS data, equivalent bands of the LandSAT TM and SPOT-XS data were used as comparison in the analysis of the spectral characteristic of MSEIS data. The latter two data sources are widely used globally for various applications. Figure 1 shows the configuration of spectral bands of the three data sets in the related electromagnetic spectrum.

Table 1. Basic Characteristic of MSEIS

No	Subjects	Characteristics
1	Number of Camera	Three cameras with electrically identical
2	Spectral Band	Near IR (0.81- 0.89 mm) Red (0.61 – 0.69 mm) Green (0.5 – 0.59 mm)
3	Optical lenses	Color corrected Nikon lenses with 75mm focal length
4	CCD Camera	Eastman Kodak KAI-1001 area array sensor; 1024x1024 pixels
5	Radiometric resolution	8 bits (256 levels)
6	Spatial Resolution	78m
7	Field of View	6.3^{o}
8	Swath width	80 x 80 km

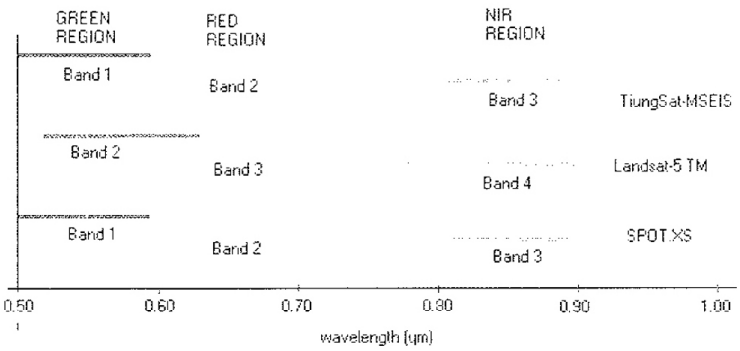

Figure 1. Spectral band configuration compared to equivalent bands of LandSAT TM and SPOT XS.

STUDY AREA

The study area was chosen on the basis of the availability of the three data sets (MSEIS, LandSAT-TM, and SPOT) within the vicinity of Johor Bahru and Changi, Singapore. For the MSEIS data, this is the only scene available for this area. The selection of this study area was also due to availability of various target types ranging from agricultural plots, urban areas and various degrees of turbidity patterns within abundant estuaries. Figure 2 shows the extend of the study area captured by the three data sets.

All the data used in this study is "raw", uncorrected for systematic and random errors in both geometry and radiometry. Sub-scening of the data were performed for the data of the respective area, resulting in different number pixels involved in all the three data sets due to different spatial resolution, with the finer (i.e. SPOT XS with 20m resolution) having the most pixels and Tiungsat-MSEIS the least.

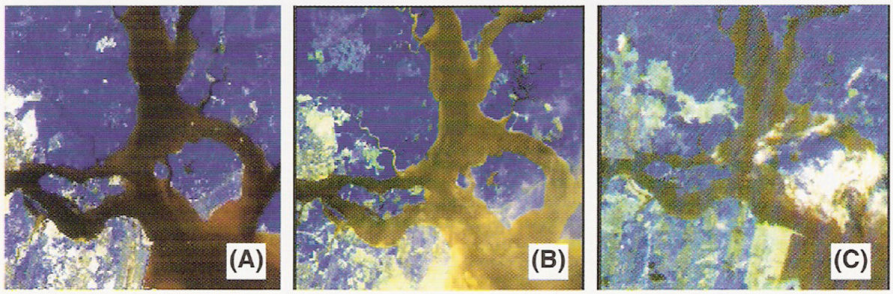

Figure 2. Study area, given by false colour composite of (a) LandSAT TM band 2, 3 and 4 in RGB , (b) SPOT XS image and (c) MSEIS image acquired for Johor Bahru area.

METHODS

In evaluating the radiometric and geometric information of MSEIS, this study focussed on the following analysis: (1) radiometric content and (2) geometric fidelity. In both analyses, comparison with the LandSAT-TM and SPOT-XS was also performed.

Radiometric Content

The content of the radiometric information of the satellite data was analysed based on: (a) univariate statistics of the data occurrence, (b) cumulative histogram, and (c) analysis of inherent noise.

(a) Univariate statistics of data occurrence

The univariate statistics of each of three data set generated could give the characteristics of pixel occurrence within the feature space. The information content can be analysed from these parameters. The most relevant parameter for information content is the dynamic range which controls the image contrast and the variation of content. A high

range of occurrence within a given allocated feature space would give a simple indication of information content, with the respective variances indicate the local variations within the image content. The largest number suggests it has the most information. Table 2 indicates the pertinent parameters of univariate statistics of the MSEIS in comparison with LandSAT TM and SPOT.

Table 2. Univariate statistics of MSEIS compared to LandSAT TM and SPOT XS

	TiungSAT-1 MSEIS			LandSAT TM			SPOT XS		
	B1	B2	B3	B2	B3	B4	B1	B2	B3
Min-max range	61 – 166	36 – 124	52 - 184	34 – 115	35 – 197	15 - 140	16 – 209	32 – 255	63 – 255
variance	194.9	194.9	258.6	67.09	322.2	1053.6	730.1	731.2	1782.5
Standard deviation	13.96	13.96	16.08	8.191	17.95	32.46	27.02	27.04	42.22

The ambiguities of MSEIS rest in the univariate statistics where all optimal values for each parameter are examined. The main reason for this is the presence of "vertical stripping" in all bands (Figure 2 (c)). Stripping within an image often indicates a malfunction of certain detectors used to capture data in a given band. In the case of MSEIS , this stripping can be avoided if the systematic mathematical model of their occurrence can be generated to eliminate these effects. However, this is not carried out due to unavailability of the sensor's data capture mechanisms. A cursory examination of the stripping also indicated the co-existence of random noises easily noted by the salt and pepper effect.

The radiometric content of the satellite image is related to the range and discernable number of discrete brightness values and is sometimes alternatively referred to as dynamic range or signal to-noise-ratio (SNR). It is expressed in terms of the number of binary digits or bits to represent the range of available brightness value in every satellite image. Within this context, the noise inherent in MSEIS again gives ambiguous optimal values.

(b) Cumulative histogram

A cumulative histogram (ch) expresses frequency of all values falling within a bin and lower in the range. The cumulative histogram is a variation of the histogram in which the vertical axis gives not just the counts for a single bin, but rather gives the counts for that bin plus all bins for smaller values of the response variable. Ch is unlike the histogram, which is a means of expressing the frequency of occurrence of values in a data set within only a series of equal ranges or bins (Richards 1995). When handling remote sensing images, it is necessary for us to use the cumulative histogram in order to pre-analyze the content of the image data before applying any image enhancement technique in the next processing stages. The ch of MSEIS is shown in Figure 3.

In Figure 3, it is clearly shown that the ch curves for MSEIS data "differs a lot" from LandSAT TM and SPOT. The low spatial resolution of MSEIS is indicated by the lowest accumulation of the graph. The peculiar shape of MSEIS cumulative histogram curves confirms the above co-existence of both systematic and random noises in the data. The direct effect of the peculiarity is an image with a low contrast (Figure 3 (c)). Supposedly, the cumulative histogram curves will look like an 'ogive' shape for a normal distribution data set, which indicates that the number of pixels count will increase by the same amount through the changes in brightness value before it saturates at a certain level.

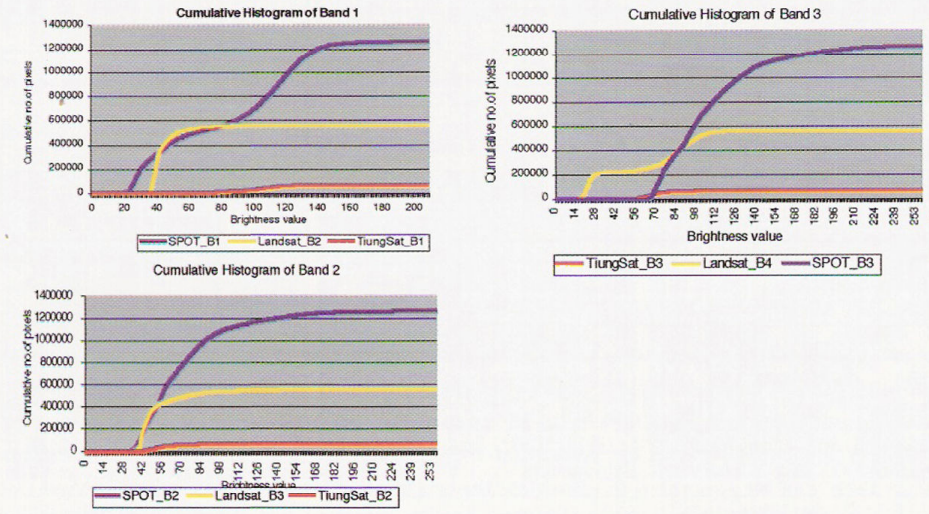

Figure 3. Cumulative histograms for all the data sets.

(c) Analysis of noise.

"Noise" refers to any unwanted disturbance affecting a measurement (as of a frequency band), especially that which degrades the information-bearing quality of the data of interest. Ideally, the radiant flux recorded by a remote sensing system in various bands is an accurate representation of the radiant flux actually leaving the feature of interest (e.g., soil, vegetation, water, or urban land cover) on the earth's surface. Unfortunately, noise can enter the data collection system at several points. For example, radiometric error in remotely sensed data may be introduced by the sensor system itself when the individual detectors do not function properly or are improperly calibrated (Jensen 1996). The intervening atmosphere between the terrain of interest and the remote sensing system can also contribute so much noise (i.e. atmospheric attenuation) that the energy recorded by the sensor does not resemble that which was reflected or emitted by the terrain.

In this study, noise is analysed using (i) expectation of pre-flight SNR values and the image appearance, and (ii) determination of incoherent noise within the data.

(i) Expected SNR

In most common remote sensing sensors, namely cameras, the SNR will be in the order of 55 dB, or a ratio of 562 : 1. That is, the signal is five hundred and sixty two times greater than the noise signal. At this ratio the noise will be unnoticeable. The following guidelines interpret some ratios of signal-to-noise in terms of the subjective picture quality. A S/N ratio of 46dB is generally accepted as the threshold at which noise can be visually seen (Table 3).

Table 3. Signal-to-noise ratio Rating

S/N ratio dB	S/N ratio:1	Picture quality
60 dB	1,000	Excellent, no noise apparent
50 dB	316	Good, a small amount of noise but picture quality good.
40dB	100	Reasonable, fine grain or snow in the picture, some fine detail lost.
30 dB	32	Poor picture with a great deal of noise.
20 dB	10	Unusable picture.

Source: http://www.cctv-information.co.uk/constant2/sn_ratio.html

The SNR of the MSEIS is given as better than 35dB at 100% and approximately 65:1. This means that the picture quality of image is in the range of reasonable to poor data quality. The visual appearance of the image reflects the SNR quality. The SNR is attributed to sensor inherent parameters such as the energy flux, altitude, bandwidth, IFOV and dwell time. Confining only these five elements, MSEIS has the longest dwell and largest IFOV which contributed significantly to noises generated in the image.

(ii) Analysis of incoherent noise

Noise in satellite data is determined using the Fourier Transform, which transforms the data in the spatial domain into frequency domain. Noise can be more easily analysed and viewed in the frequency domain rather than its original form. In this study a sub-scene over water-covered areas of the three data sets were analysed for this purpose. The main reason for choosing this target is because of homogeneous pattern of a water body would give a better noise pattern against the background. Figure 4 shows the results of Fourier transforms of the data sets. Evidence of systematic noise within MSEIS data is shown by the frequency occurrence on the vertical and aligned axes. The bright spot off these two main axes formed can be associated with the random noises. Stripping occurrence in band 3 is more severe than band 1 and 2, thus contributing to the periodic noises in the data. In comparison for LandSAT TM and SPOT, both the random and systematic noises inherent in the data sets were found to be less than MSEIS, as expected due to their superior SNR elements, namely dwell time and spatial resolution. The MSEIS characteristics would have been even poorer if put to the orbit at the same altitude as LandSAT and SPOT. This noise appears in channel 2 in the diagonal direction, similarly with channel 1 as shown in Figure 4, respectively.

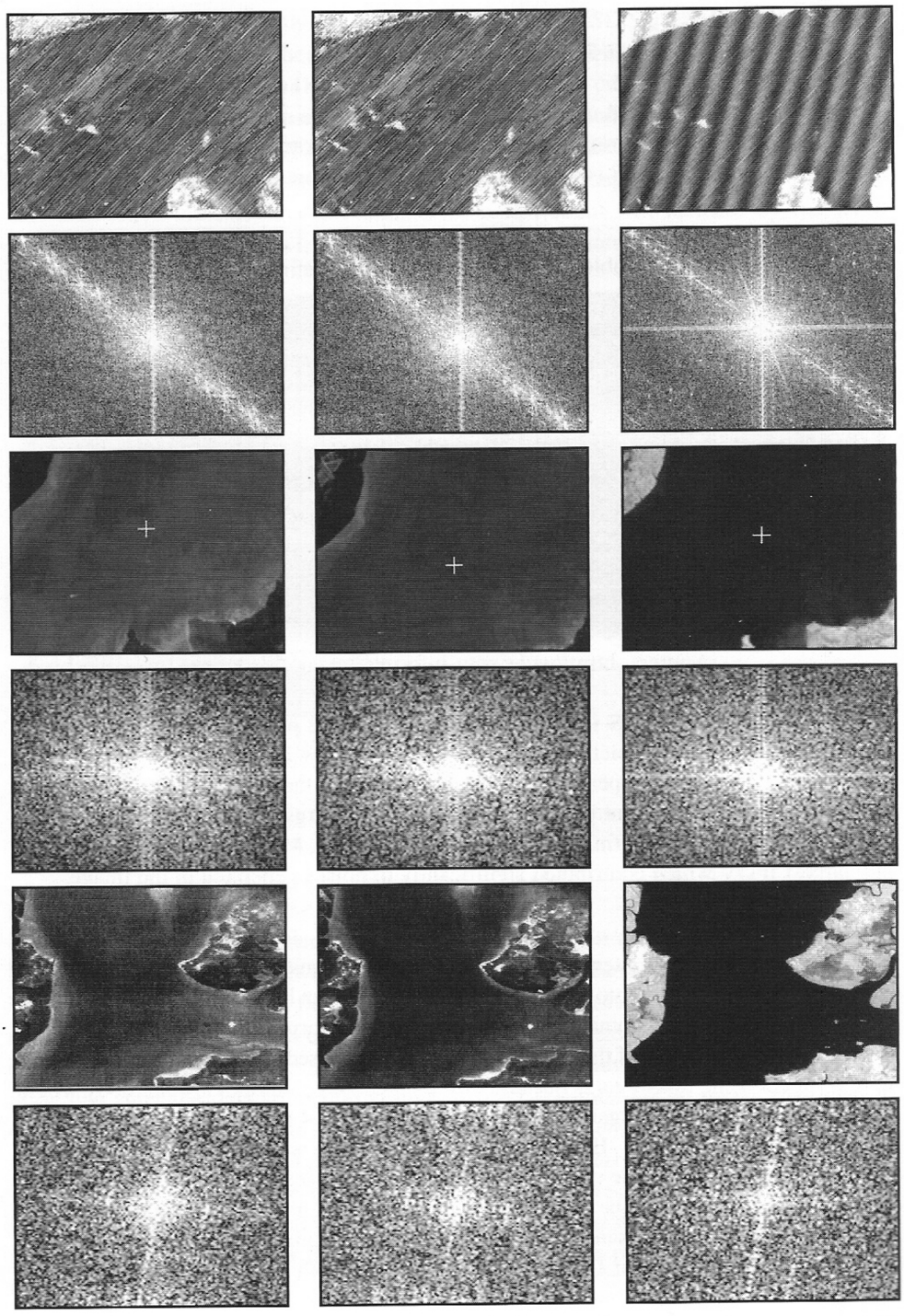

Figure 4. The Fourier transforms of : (a) MSEIS, (b) LandSAT TM and (c) SPOT XS

GEOMETRIC FIDELITY

Digital images can be thought of as a regular grid of normally square pixels. The pixel shape is generally assumed to be square by most computer image processing programs, which may not be the case with raw data. The degree of distortion depends on the type of sensor and platform, the width of the view angle or field of view and the altitude of the platform. Any remote sensing image, regardless of whether it is acquired by a multi spectral scanner on board a satellite like LandSAT TM (across-track scanning systems), SPOT (pushbroom scanning system) and MSEIS (snapshot system), will have various geometric distortions.

An along-track scanner (pushbroom system) has no scanning mirror and there is a fixed geometric relationship among the CCD detector elements recording each scan line. In essence, the geometry of each scan line of an along-track scanner image is similar to that of an aerial photograph. Line to line variation occurs according to the altitude or attitude (angular orientation) of the spacecraft along the flight line. Often, on-board gyroscopes and the GPS system are used to measure these variations and geometrically correct the data from along-track scanners (Lillesand *et* al 1994). Images from LandSAT TM (across-track scanning systems) exhibit two main types of geometric distortion. They too exhibit relief displacement, similar to aerial photographs, but in only one direction parallel to the direction of scan. There is no displacement directly below the sensor, at nadir. As the sensor scans across the swath, the top and side of objects are imaged and appear to lean away from the nadir point in each scan line. Again, the displacement increases, moving towards the edges of the swath. The MSEIS with the CCD-based sensor, although with different data capture mechanism, hypothetically would have nearly similar geometry characteristics. In this study, the geometric fidelity, as viewed by its accuracy, can be achieved in minimising the distortions found in the image using the same number and configuration of ground control points (GCPs).

Geometric Distortion

Depending on the distortion in the imagery, the number of ground control points (GCPs) used and the degree of topographic relief displacement in the area, higher-order polynomial equations may be required to geometrically correct the data. The order of the rectification is simply the highest exponent used in the polynomial. Generally, for moderate distortion in a relatively small area of an image a first-order, six-parameter, a fine transformation is sufficient to rectify the imagery to a geographic frame of reference (Jim 2001).

Before applying the rectification to the entire set of data, it is important to determine how well the six coefficients derived from the least square regression of the initial GCP account for the geometric distortion in the input image. The method used most often involves the computation of the root-mean- square error (RMS) for each of the ground control point. The square root of the squared deviations represent a measure of the accuracy of this GCP in the image. By computing RMS error for all GCP, it is possible to see which GCPs exhibit the greatest error and then sum all the RMS error. This in return could give the accuracy of geometric correction that can be achieved by the respective data and hence can be a good representation of the data geometric fidelity.

Given that the data is raw, untreated for both systematic and random distortions, this study assumes that the minimization would also normalise the systematic errors. For this the polynomial transformation will be used. Measurement techniques to correct these errors involve the collection of GCPs distributed evenly over the whole image. The best GCPs are located at well- defined and easy to recognize points on both the georeferenced (being registered to) and uncorrected (being registered) data sets. The displacements of these GCPs between the uncorrected and georeferenced data sets are used in the correction of these errors. A least squares regression analysis is used to determine the coefficients for two coordinate transformation equations which relate the distorted image to the desired true map projection.

Residuals

If the orientation of the GCPs in the map is slightly different than in the image (due to real distortion or measurement error), the new transformed image coordinates will not exactly coincide with the chosen GCPs on the map. This difference is known as a *residual*. If the residual for any one point is much larger than the others, a measurement error is often the case (Bernstein 1983).

The concept of residuals can be shown easily using a line of best fit in a two-dimensional graph. Figure 5 shows a series of points with a first, second and third order line-of-best-fit. The fit, in this case, was done to minimize the distance in y from the line to each point. The difference between the predicted value (the line) and the actual point is known as the residual or error. Note that in this case, the third order line-of-best-fit has a greater error than the second order line (Fogel 2001).

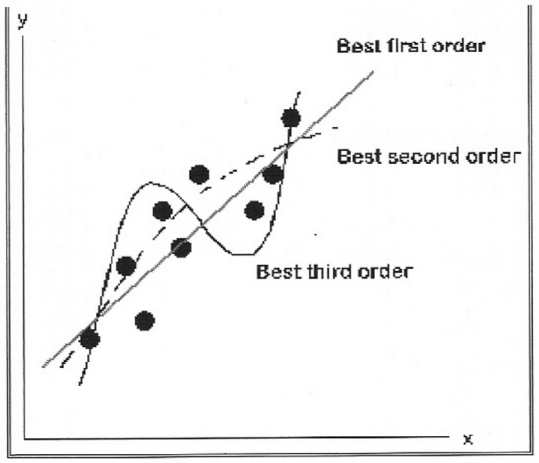

Figure 5. A figure showing lines-of-best-fit regression only *(Source: Jim 2001)*

In the image, this residual is an error between the location of a known GCP and the value calculated from the transformation equation. In some cases the use of a very high order equation could be used to fit the new image almost exactly to the coordinates, the precision associated with that might be spurious. Not only is it expected that there is some measurement error associated with the GCP location coordinates, but high order

equations can become unpredictable between control points, actually increasing error away from the GCPs. The RMS error is a common means of reporting error in a transformed image (Lillesand and Kiefer 1994; Bernstein 1983). RMS error is the distance between the map coordinates of the GCPs and the transformed coordinates of the GCPs.

In this study two set of GCPs were established, Set 1 known as control points used for geometric correction and the second, Set 2, the check points were used in determining the accuracy analysis, namely the rmse. Figure 6 shows the configuration of these points. The transformation functions examined were polynomial (1st to 3rd order). The rmse of each transformation are listed in Table 4. The second step of geometric correction is the resampling process. Three resampling approaches were used here, ie. Nearest neighbour, cubic bilinear and cubic convolution, using the same configuration of GCPs and the same geometric corrections. Apart from rmse of the geometrically data, we also determined the known distance (Figure 7) from the three resampling techniques to analyse the effect of the resampling to the distortions. Table 5 summarises the discrepancy/distortions due to different resampling approaches employed. To confirm the rmse and distortions analysed in the above, an analysis of polynomial fit was also carried out. A polynomial fit is used to estimate the amount of scaling in x and y, rotation, offset in x and y, and non-orthogonally angle associated with a terrain corrected image.

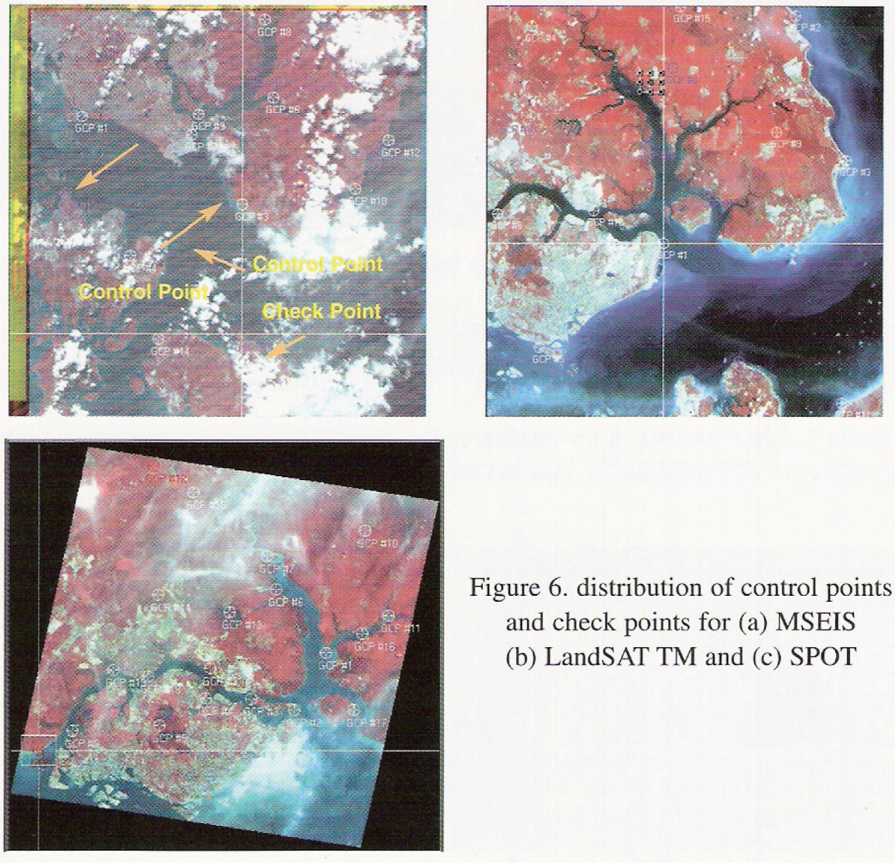

Figure 6. distribution of control points and check points for (a) MSEIS (b) LandSAT TM and (c) SPOT

Table 4. Root Mean Square Error (RMSE) in pixels for each dataset

		MSEIS	SPOT	LandSAT TM
1st degree of polynomial	Total control point error	1.7251	0.3039	1.2396
	Total check point error	2.5231	2.1923	1.9586
2nd degree of polynomial	Total control error	0.3857	0.3644	0.2888
	Total check point error	1.9339	1.5339	0.6114
3rd degree of polynomial	Total control point error	0.4079	0.2857	0.2077
	Total check point error	1.7342	1.5834	0.6337

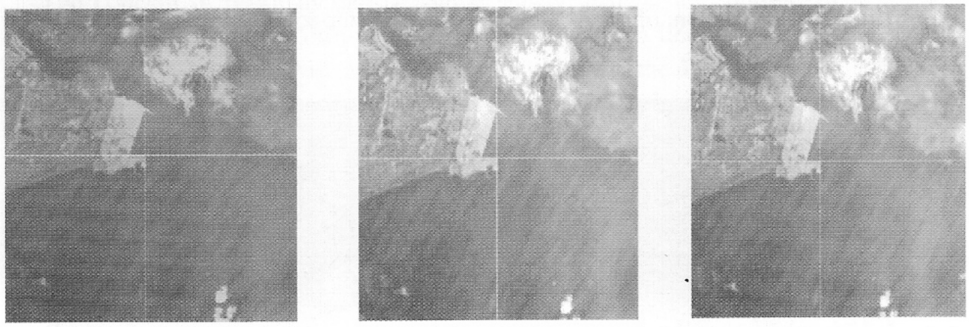

Nearest Neighbour Bilinear Interpolation Cubic Convolution

Figure 7. Resampling technique using Nearest Neighbour, Bilinear Interpolation and Cubic Convolution

Table 5. Discrepancies of the geometrically corrected due to different resampling techniques in TM and MSEIS data: (a) the x and y offset, and (b) differential distance.

(a)

1st order polynomial transformation	Nearest Neighbour		Bilinear Interpolation		Cubic Convolution	
Differential coordinate	Δx	Δy	Δx	Δy	Δx	Δy
MSEIS	20.124	10.036	70.039	10.314	30.378	40.447
LandSAT TM	20.301	10.016	20.134	25.146	21.012	23.044

(b)

1st order polynomial transformation	Differential distance (m) Nearest Neighbour	Bilinear Interpolation	Cubic Convolution
MSEIS	22.4877	70.7943	50.5844
LandSAT TM	22.6753	32.2133	31.2056

The polynomial fit analysis is given by the following equations (Anon 1998):

$x_o = a + b\,x_i + c y_i$
$y_o = d + e\,y_i + f\,y_i$
where,

x_o = output projection x coordinate (measured)
y_o = output projection y coordinate (measured)
x_i = input projection x coordinate (truth)
y_i = input projection y coordinate (truth)
a, b, c, d, e, f are transformation coefficients

The polynomial coefficients were determined from a least squares fit of the x and y coordinates of features located in the geometrically corrected data and their corresponding x and y coordinates for the same feature in the ground control source. The error or distortion can be expressed as scale errors in the x and y directions, and rotation angles in the respective axes. Both the scale errors (Sx, Sy) and angles (theta, alpha) are determined from the polynomial transformation coefficients by the following:

$$S_X = \frac{\sqrt{e^2 + f^2}}{bf + ce}$$

$$Sy = \frac{\sqrt{b^2 + c^2}}{bf + ce}$$

$$\theta \quad \tan^{-1}\left(\frac{e}{f}\right)$$

$$\_ = \tan^{-1}\left(\frac{-be - cf}{bf - ce}\right)$$

where,

S_X = scale error in x direction,

S_y = scale error in y direction,
_ = non-orthogonality angle,
θ = rotation angle,
a = offset in x direction,
d = offset in y direction and,
a, b, c, d, e, f are transformation coefficients

The scale error can be converted to pixels by the following:

$(S_x\text{-}1)$ x (image pixel size in x)
$(S_y\text{-}1)$ x (image pixel size in y)

θ can be converted to pixels by the following:

θ x (size of image diagonal)

where

size of image diagonal = $\sqrt{(image\ pixel\ size\ x)^2 + (image\ pixel\ size\ y)^2}$

Table 4 shows that the MSEIS has the same geometric quality as SPOT and LandSAT. This is evidenced by the rmse of the accuracy achieved in the geometric correction. This is not as expected as normally low spatial resolution usually have poor rmse due to the difficulty in pointing GCPs. Although the MSEIS is the worst in the reported rmse, the results are comparable with those data at similar resolution, such LandSAT MSS. Table 5 confirms the distortion pattern observed in Table 4, where MSEIS discrepancies for known distances in the geometrically corrected data are similar to the LandSAT TM. The magnitude of discrepancies in MSEIS shown in Table 6 is influenced by the resampling technique chosen, and careful selection of this technique would reduce the error by about 50%.

Table 6. Distortion error from data SPOT, LandSAT TM and MSEIS by polynomial fit.

Polinomial fit parameters	SPOT	LandSAT TM	MSEIS
S_x	1.003442904	0.527	0.51767
S_y	-0.19587	10.47429	44.265
theta	-2.1183	1.8327	-77.32
alpha	0.06885808	14.19	38.5764
Scale error in image pixel size in y	0.0704	-20.506	10.464
Scale error in image pixel size in x	0.06885808	14.19	35.5864

The polynomial fit analysis (Table 6) indicates that the amount of errors in the x and y directions of the LandSAT TM and MSEIS share the same pattern of the scale errors in y axis. SPOT data on the other hand has few scale errors and is symmetrically distributed across the image. In terms of rotation or angular errors, the reported theta and alpha clearly show similar patterns of scale errors in both LandSAT TM and MSEIS. Total accumulated scale errors in Table 6 indicate that some form of pre-processing of the geometric data, especially for systematic errors, has been carried on the SPOT data prior to dissemination to users.

CONCLUSION

This study was undertaken with the aim of analysing the radiometric and geometric content of MSEIS. In particular, the radiometric analysis focussed on signal-to-noise ratio and incoherent noise while the geometric studies focussed on geometric fidelity. Comparison of MSEIS with equivalent bands of the LandSAT TM and SPOT was also performed. Results indicate that the TiungSAT-1 MSEIS radiometric content is significantly disturbed by incoherent noises both at systematic and random levels. However, for geometric fidelity, the MSEIS exhibits remarkably good performance which is comparable to LandSAT TM despite its much lower resolution. This is attributed to the CCD-based sensor which is well known for its sensitivity to spatial patterns.

The poorer SNR performance of MSEIS when compared to LandSAT TM and SPOT XS is expected because the MSEIS is using an off-the-shelf camera while the LandSAT TM and SPOT XS cameras are custom-built. Nevertheless, TiungSAT-1 can be usefully exploited for bathymetric studies, geological interpretation, and land use applications.

ACKNOWLEDGEMENTS

The authors would like to thank Year 4 remote sensing students at UTM for collecting ground control points for preparing this paper.

REFERENCES

Anon 1998 ."Geometric Algorithm Theoretical Basis Document". *Image Assessment System*

Bernstein, R 1983. "Image Geometry and Rectification". Chapter 21 in *The Manual of Remote Sensing*, 2nd Edition New York: American Society of Photogrammetry

Fogel, D. N. 2001. "Image Rectification with Radial Basis Functions: Application to RS/GIS Data Integration"http://www.ncgia.ucsb.edu/conf/SANTA_FE CD-ROM/sf_papers/ fogel_david/ santafe. html (26th July 2001)

Jensen, J.R. 1996. *'Introductory Digital Image Processing* ', pg 40-49, 77-85,116-121.

Jim, Y 2001. "Lecture Note Chapter 1 - Image Geometry" http://astro1.chungnam.ac.kr/~yjim/rsnote/geometry/GEOM.htm (26th July 2001)

Lillesand, T. M. and Kiefer, R. W. 1994. "*Remote Sensing and Image Interpretation.*" 3rd Edition. New York: John Wiley & Sons, Inc.